Journal of
Marine Science and Engineering

MDPI

Article

An Improved VMD–EEMD–LSTM Time Series Hybrid Prediction Model for Sea Surface Height Derived from Satellite Altimetry Data

Hongkang Chen [1,2], Tieding Lu [1,2], Jiahui Huang [3,*], Xiaoxing He [3] and Xiwen Sun [1,2]

1 School of Surveying and Geoinformation Engineering, East China University of Technology, Nanchang 341000, China; chk@ecut.edu.cn (H.C.); tdlu@ecut.edu.cn (T.L.); xwsun@ecut.edu.cn (X.S.)
2 Key Laboratory of Mine Environmental Monitoring and Improving around Poyang Lake of Ministry of Natural Resources, East China University of Technology, Nanchang 330013, China
3 School of Civil and Surveying & Mapping Engineering, Jiangxi University of Science and Technology, Ganzhou 341000, China; xxh@jxust.edu.cn
* Correspondence: hjh@mail.jxust.edu.cn

Abstract: Changes in sea level exhibit nonlinearity, nonstationarity, and multivariable characteristics, making traditional time series forecasting methods less effective in producing satisfactory results. To enhance the accuracy of sea level change predictions, this study introduced an improved variational mode decomposition and ensemble empirical mode decomposition–long short-term memory hybrid model (VMD–EEMD–LSTM). This model decomposes satellite altimetry data from near the Dutch coast using VMD, resulting in components of the intrinsic mode functions (IMFs) with various frequencies, along with a residual sequence. EEMD further dissects the residual sequence obtained from VMD into second-order components. These IMFs decomposed by VMD and EEMD are utilized as features in the LSTM model for making predictions, culminating in the final forecasted results. The experimental results, obtained through a comparative analysis of six sets of Dutch coastal sea surface height data, confirm the excellent accuracy of the hybrid model proposed (root mean square error ($RMSE$) = 47.2 mm, mean absolute error (MAE) = 33.3 mm, coefficient of determination (R^2) = 0.9). Compared to the VMD-LSTM model, the average decrease in $RMSE$ was 58.7%, the average reduction in MAE was 60.0%, and the average increase in R^2 was 49.9%. In comparison to the EEMD-LSTM model, the average decrease in $RMSE$ was 27.0%, the average decrease in MAE was 28.0%, and the average increase in $R2$ was 6.5%. The VMD–EEMD–LSTM model exhibited significantly improved predictive performance. The model proposed in this study demonstrates a notable enhancement in global mean sea lever (GMSL) forecasting accuracy during testing along the Dutch coast.

Keywords: sea level change; deep learning; time series prediction; VMD; EEMD; LSTM

Citation: Chen, H.; Lu, T.; Huang, J.; He, X.; Sun, X. An Improved VMD–EEMD–LSTM Time Series Hybrid Prediction Model for Sea Surface Height Derived from Satellite Altimetry Data. *J. Mar. Sci. Eng.* **2023**, *11*, 2386. https://doi.org/10.3390/jmse11122386

Academic Editors: João Miguel Dias and Chung-yen Kuo

Received: 7 November 2023
Revised: 1 December 2023
Accepted: 15 December 2023
Published: 18 December 2023

1. Introduction

In recent years, the increasing rise in sea level has had severe social impacts on coastal areas, including the degradation of freshwater resources, damage to infrastructure, and the depletion of agricultural resources [1,2]. The Sixth Assessment Report of the Intergovernmental Panel on Climate Change (IPCC) highlighted that under the influence of human activities, the rate of the rise in sea level has been steadily accelerating. Between 1901 and 1971, the average rate of the rise in sea level was 1.3 mm per year, which increased to 1.9 mm per year between 1971 and 2006 and rose further to 3.7 mm per year between 2006 and 2018 [3]. To address the threats posed by rising sea level worldwide, accurate predictions of future changes are of paramount importance for the sustainable development and protection of coastal regions [4].

There are two main categories of methods used for predicting sea level in time series forecasting: statistical methods and machine learning methods [5,6]. Statistical methods are commonly employed in time series forecasting and are rooted in the core concept of conducting statistical analyses on historical data to capture the patterns and trends for predictive purposes [7,8]. Representative models in this category include autoregressive integrated moving average (ARIMA) and exponential smoothing [9,10]. However, these models encounter difficulties in handling complex nonlinear data due to the need for manual feature selection and parameter adjustments, which result in certain limitations [11,12]. Comparatively, machine learning models demonstrate more flexible adaptation by learning adaptively from nonlinear relationships in the data to capture underlying patterns more efficiently and exhibit superior predictive performance especially when dealing with complex time series [13].

Currently, machine learning time series prediction includes various methods such as support vector regression (SVR), decision tree (DT), neural network (NN), and hybrid models [14–18]. Among these methods, neural networks, by virtue of their special network architecture and feature extraction methods, show strong generalization ability and adaptability to complex data and are more and more widely used in sea level time series forecasting with nonlinear, nonsmooth, and multivariate attributes [19–22]. Makarynskyy et al. (2004) utilized artificial neural networks (ANNs) to perform multistep predictions based on measured sea level data from a tidal station in Australia, demonstrating the feasibility of using neural network methods in sea level prediction [23]. Nezhad et al. (2023) applied neural networks to storm surge flood modeling and demonstrated that neural networks have great potential to improve model accuracy and reliability [24].

In the field of neural network prediction, long short-term memory (LSTM) networks have shown significant advantages in long-period time series prediction with their superior adaptive learning ability and memory module, especially standing out in sea level time series prediction. Alenezi et al. (2023), by utilizing the powerful data learning and processing of nonlinear correlations of neural networks, applied the LSTM model to sea level data interpolation and Mina Salman sea level prediction with satisfactory results [25]. Balogun and Adebisi (2021) conducted comprehensive predictions and comparisons of changes in sea level along the west coast of Peninsular Malaysia using three models: ARIMA, SVR, and LSTM. Their results validated the ability of the LSTM model in predicting sea level [26]. Therefore, in this paper, the LSTM model is chosen as the prediction model in the hybrid model.

Given the excellent performance of neural networks in time series forecasting, various time series forecasting fields have been applied to the field of mixed model forecasting by combining them with techniques such as data decomposition [27–29]. De Siqueira et al. (2021) verified the feasibility of combining neural networks with hydrodynamic models to reduce errors in sea level change bands by updating the output of a hydrodynamic model (Hycom) with a neural network in order to perform an error correction for this combined method [30]. Song et al. (2022) conducted multifaceted comparisons of various data decomposition methods, such as complementary ensemble empirical mode decomposition (CEEMD), time-varying filtering-based empirical mode decomposition (TFV–EMD), wavelet transform (WT), and the fusion of these methods with the Elman neural network (ENN) in minute-scale time series predictions of sea level. Their study confirmed that the TVF–EMD–ENN model exhibits the best predictive performance [31]. Wang et al. (2021) incorporated time series of wind speed that had been secondarily decomposed using CEEMD and wavelet packet decomposition (WPD) into a gated recurrent unit (GRU) for making predictions of short-term wind speed [32].

Variational mode decomposition (VMD), as an emerging data decomposition technique, has stood out among the various decomposition methods due to its unique nonrecursive variational approach and exceptional decomposition capability. It has been extensively utilized in the field of mixed deep learning time series prediction [33,34]. Wang et al. (2020) combined the VMD–LSTM model and used an improved particle swarm optimization algorithm (IPSO) to optimize model parameters, confirming the higher predictive accuracy of the VMD–LSTM model in photovoltaic short-term power time series prediction [35].

Huang et al. (2022) compared empirical mode decomposition (EMD) and VMD. They found that VMD had better noise removal capabilities and verified the higher precision of the VMD-LSTM model in predicting variations in coal thickness [36]. Han et al. (2019) performed multifaceted comparisons of various prediction models, including VMD–LSTM, persistence (PER), wavelet (WT), and BP neural networks. Their research validated that the VMD–LSTM model exhibited higher accuracy in wind power prediction [37].

The studies mentioned above, conducted in various domains of time series analysis, have consistently shown that the VMD-LSTM model has superior predictive accuracy. However, in practical applications, due to variations in VMD parameter settings and data characteristics, incomplete VMD may occur. This results in residual components that still contain a certain level of fluctuations and nonwhite noise elements. This inadequately processed information can potentially have a detrimental impact on the predictive accuracy of the VMD–LSTM model, particularly in forecasting complex nonlinear and irregular time series.

In light of the aforementioned challenges, this paper addresses the differences in prediction accuracy under the LSTM model by comparing the values of each intrinsic mode function (IMF) and residual terms obtained from four different decomposition methods: VMD, EMD, ensemble empirical mode decomposition (EEMD), and complete ensemble empirical mode decomposition with adaptive noise (CEEMDAN). An improved variational mode decomposition and ensemble empirical mode decomposition–long short-term memory (VMD–EEMD–LSTM) is proposed. In this model, the optimal value of K for VMD is determined using the signal-to-noise ratio method. Subsequently, noise analysis is performed on the decomposed residuals, and those residuals with nonwhite noise are further decomposed using EEMD. The modal components with the number of modal components greater than K after EEMD are fused to improve the prediction accuracy of the model and minimize the model complexity. Finally, the sequences obtained from each decomposition are input as feature values into the LSTM model for training. The prediction was performed after adjusting the hyperparameters of the LSTM model to the optimal parameters. The model not only retains the advantages of the original VMD-LSTM model in the prediction accuracy of each IMF but also integrates the advantages of the EEMD-LSTM model in the residual term and the overall prediction accuracy, which further improves the prediction accuracy of the sea level time series. In the experiments of this paper, the prediction accuracy of the VMD-EEMD-LSTM model is comprehensively analyzed by comparing different deep learning models, multiple data decomposition methods, and satellite altimetry data from different virtual coast altimetry stations. By developing this one improved deep learning hybrid prediction model, this study not only introduces a new perspective to the field of hybrid deep learning models for second-order decomposition but also provides a new method for solving the problem of high-accuracy sea level time series prediction.

2. Principles and Methods

2.1. Signal Processing Methods

VMD, EMD, EEMD, and conformal empirical mode decomposition with adaptive noise (CEEMDAN) are all widely used adaptive methods of data decomposition in the fields of signal processing and data analysis [38–40]. Among the various methods, VMD stands out as a fully nonrecursive modal decomposition method. Its core idea involves modeling a signal as a variational problem and subsequently seeking the optimal solution through iterative transformations. Ultimately, this process decomposes nonstationary signals into a series of standard orthogonal modal functions. The corresponding principles are as follows [41].

With the objective of minimizing the summation of the estimated bandwidths for each modal component $\mu_K(t)$, a constrained variational problem model is aimed at identifying the optimal solution. The specific formulation of the constrained variational problem model is provided below.

$$\begin{cases} \min_{\{\mu_K\},\{\omega_K\}} \left\{ \sum_K \left\| d_t \left[\left(\delta(t) + \frac{j}{\pi t} \right) * u_K(t) \right] e^{-j\omega_K t} \right\|_2^2 \right\} \\ s.t. \sum_K \mu_K = f \end{cases} \tag{1}$$

In Equation (1), $j^2 = -1$, $\delta(t)$ represents the Dirac function, $\{\mu_K\}$ corresponds to the modal functions obtained after decomposition, $\{\omega_K\}$ denotes the central frequencies associated with each mode, and f represents the original signal.

In order to achieve the best possible solution for the constrained variational problem, the introduction of quadratic penalty factors α and Lagrange multiplier operators λ_t transforms the problem into an unconstrained variational problem.

$$L(\{\mu_K\},\{\omega_K\},\lambda) = \alpha \sum_K \left\| \partial_t \left[\left(\delta(t) + \frac{j}{\pi t} \right) * \mu_K(t) \right] e^{-j\omega_K t} \right\|_2^2 + \left\| f(t) - \sum_K \mu_K(t) \right\|_2^2 + \langle \lambda(t), f(t) - \sum_K \mu_K(t) \rangle \tag{2}$$

where $L(*)$ represents the augmented Lagrangian function, $\left\| f(t) - \sum_K \mu_K(t) \right\|$ is the quadratic penalty term. Subsequently, an alternative direction method with multiplier operators is used to solve the unconstrained variational problem, and the optimal solution is obtained by alternating updating ${\mu_K}^{n+1}$, ${\omega_K}^{n+1}$, and λ^{n+1}.

The EMD method is a recursive method that breaks down the data into a finite number of intrinsic mode functions (IMFs). These IMFs represent the underlying properties of the time series signals, along with a residual sequence [42]. However, the EMD may suffer from the mode-mixing problem in the IMF sequences. To overcome this challenge, this study introduced the EEMD method. EEMD gradually introduces normally distributed white noise into the original signal and then offsets this noise through multiple averaging calculations. This process leads to more precise decomposition of the signal and effectively avoids the mode-mixing phenomenon that can occur during the EMD process [43,44]. The specific process is as follows:

(1) Initially, white noise denoted as $\omega(t)$ is introduced into the original signal $x(t)$.

$$x_i(t) = x(t) + \omega_i(t), i = 1, 2, \ldots, m \tag{3}$$

(2) Subsequently, the EMD method is employed to decompose the initial noisy signal, resulting in n IMFs, represented as $C_i(t)$, and a residual sequence represented as $r_i(t)$.

$$x_i(t) = \sum_{j=1}^{n} C_{ij}(t) + r_i(t) \tag{4}$$

(3) Steps (1) and (2) are iteratively executed for a total of m times, in which white noise is added and IMF components are obtained through decomposition in each iteration. Finally, all the components obtained from the IMFs are integrated and averaged to obtain the ultimate result of EEMD signal decomposition.

CEEMDAN introduces an adaptive noise complete set to automatically construct noise components, enabling more effective extraction of modal components in the signal compared to EEMD. This enhances the accuracy and robustness of data decomposition [45].

2.2. Long Short-Term Memory

LSTM is an improved type of recurrent neural network (RNN). Its distinctive memory module is beneficial for handling long-term dependencies and mitigating the challenges related to vanishing and explosion gradients [46]. Compared with traditional neural networks, LSTM networks exhibit pronounced advantages when addressing tasks pertaining to the prediction of lengthy time series data. Consequently, LSTM networks find extensive applications in domains such as time series forecasting [47,48].

The architectural framework of an LSTM network comprises an input layer, intermediate hidden layers, and an output layer. Each hidden layer manages the storage and retrieval of data using input, forget, and output gates, as shown in Figure 1.

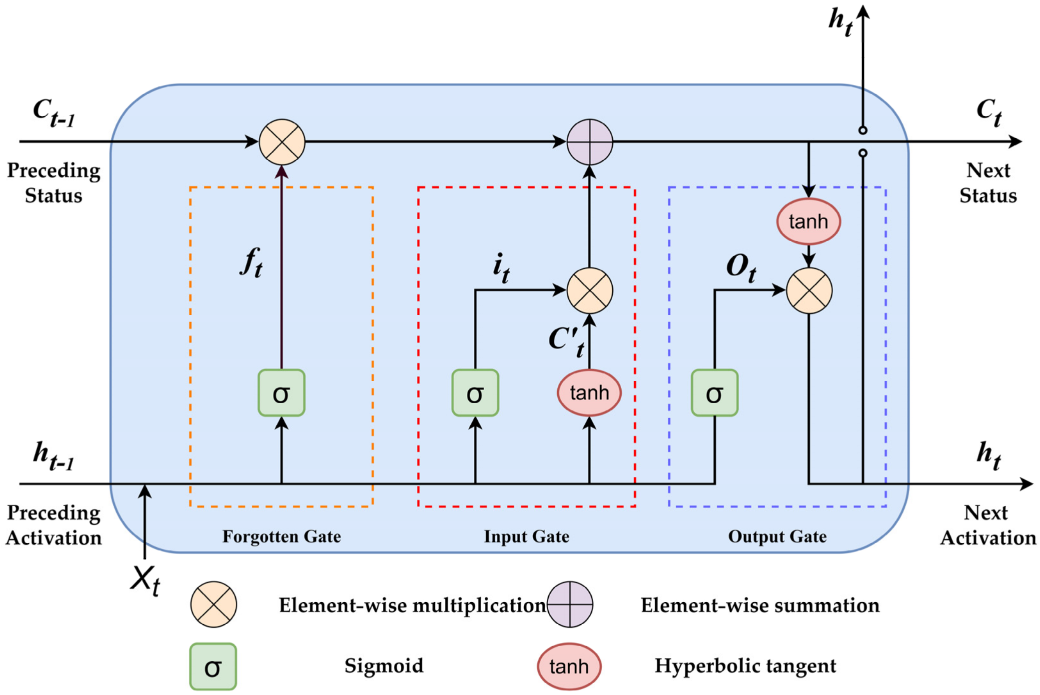

Figure 1. Basic structure of LSTM.

As illustrated in the figure, LSTM processes the input of high-temporal data related to sea surface elevation and the previous moment's hidden state output using three gates. The primary process is as follows [49]:

(1) LSTM, through the forget gate (denoted as f_t), determines whether to discard or retain information related to X_t and h_{t-1} is governed by the activation function σ of the forget gate.

$$f_t = \sigma(W_f \cdot [h_{t-1}, X_t] + b_f) \tag{5}$$

In the equations, W and b represent the weight matrices and biases, respectively. f_t is a vector with values in the range of 0 to 1, where the values within the vector indicate whether information in the cell state C_{t-1} is preserved. A value of 0 implies no preservation, while 1 implies full preservation.

(2) The cell state is updated through the input gate by passing X_t and h_{t-1} to the activation function σ to determine the information update.

The tanh function is applied to X_t and h_{t-1} to generate a new vector C'_t (where C'_t is a vector in the range of -1 to 1), and the tanh output is multiplied by σ output.

$$i_t = \sigma(W_i \cdot [h_{t-1}, X_t] + b_i) \tag{6}$$

$$C'_t = \tanh(W_c \cdot [\mathrm{h}_{t-1}, X_t] + b_c) \tag{7}$$

(3) The cell state from the previous layer is element-wise multiplied with the forget vector, and then this value is element-wise added to the output of the input gate, resulting in the updated cell state.

$$C_t = f_t * C_{t-1} + i_t * C\prime_t \tag{8}$$

In the equations, $f_t * C_{t-1}$ determines the forgetting of information in C_{t-1}, while $i_t * C_t'$ determines the addition of information in C_t' to the new memory cell state C_t.

(4) Through the output gate O_t, the value of the next hidden state h_t is determined, and this hidden state contains information from previous inputs.

$$O_t = \sigma(W_O \cdot [h_{t-1}, X_t] + b_O) \quad (9)$$

$$h_t = O_t * \tanh(C_t) \quad (10)$$

2.3. The VMD–EEMD–LSTM Hybrid Second-Order Decomposition Prediction Model

VMD and EEMD, as two classical data-processing methods, have been widely applied in hybrid modeling. Their effectiveness in enhancing the predictive accuracy of deep learning models has been well established [50,51]. The VMD-LSTM model is a popular hybrid deep learning approach that has been extensively used for time series forecasting. Its applications encompass load forecasting and wind speed prediction, where it has showcased remarkable performance [52,53]. The VMD–LSTM model leverages VMD to perform decomposition of the initial data into a sequence of IMFs and a residual sequence. Subsequently, the model individually forecasts each IMF sequence and the residual sequence using the LSTM model. Ultimately, the predicted outcomes of each sequence are aggregated to derive the final model prediction. During the prediction process, as the standard normal mode functions obtained through VMD are stationary signals, predicting each IMF separately can achieve higher prediction accuracy.

In the end, the predicted outcomes of each sequence are combined to determine the final model prediction. When making predictions, it is more accurate to predict each IMF separately since the standard normal mode functions obtained through VMD are stationary signals. However, in practical VMD, the residual sequence still contains some fluctuating characteristics and high-frequency noise, and their values are relatively large. If these parts of the data are not appropriately processed, they will adversely affect the overall predictive accuracy of the model [54–56]. In contrast, the EEMD–LSTM model is a recursive decomposition method, and its main predictive errors are concentrated in the IMF components, which perform well in predicting the residual sequence and overall data. Based on this, this study proposed a deep learning hybrid model called VMD–EEMD–LSTM. This model employs VMD for the initial data decomposition and then utilizes EEMD to further break down the residual components with lower prediction accuracy resulting from the VMD. Subsequently, each IMF obtained through both VMD and EEMD is used as a feature used as input into the LSTM model for making predictions. Ultimately, the forecasted outcomes of each IMF are aggregated to yield the model's comprehensive prediction. This approach augments the overall predictive precision of the model by handling the residual components produced by VMD. The detailed procedure is elucidated in Figure 2.

The specific process for predicting using the mixed VMD-EEMD-LSTM second-order decomposition model is as follows:

Step 1: Preprocess the time series data on sea level from each station and then input them into the VMD model (with K as the number of components in the model) for decomposition.

Step 2: Take the residual sequence "Residual $_1$" obtained from the VMD and input it into the EEMD model for further decomposition. This will yield various model components as well as "Residual $_2$".

Step 3: Through extensive experiments, it has been determined that among the IMF components obtained through EEMD, the IMFs after IMF$_K$ (IMF $_{K+1}$ to IMF $_\mathrm{n}$) and "Residual $_2$" have smaller prediction errors. To mitigate experimental intricacies and guarantee the precision of the model's predictions, the IMF components beyond IMF$_K$ and "Residual $_2$" are combined and utilized as input features for the LSTM model to facilitate the prediction process.

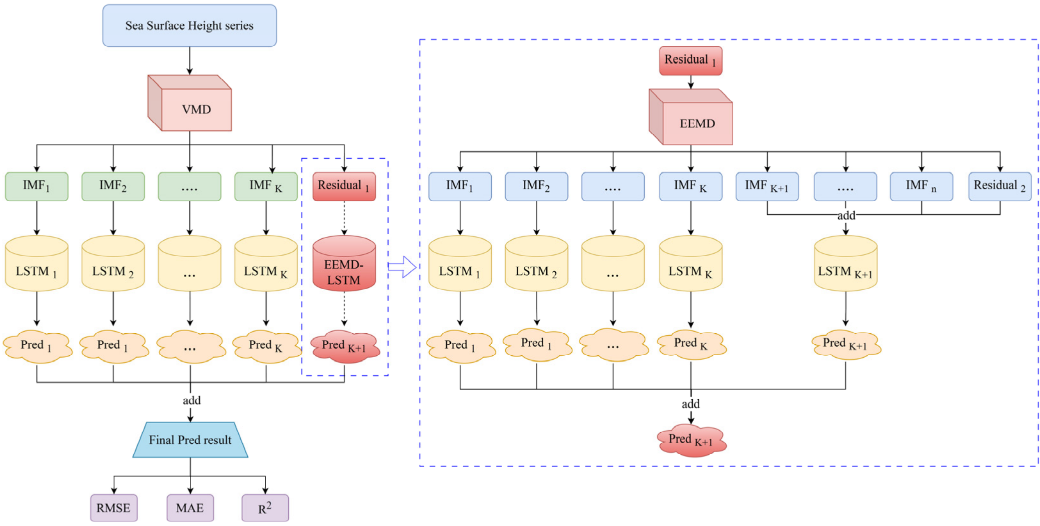

Figure 2. The mixed VMD–EEMD–LSTM second-order decomposition model.

Step 4: Utilizing the distinct IMF components acquired from both VMD and the EEMD as distinct features, these components are fed into the LSTM model for prediction purposes. This process yields a total of $2K + 1$ predictions.

Step 5: Aggregate and amalgamate the $2K + 1$ predictions to derive the ultimate prediction generated by the VMD–EEMD–LSTM model.

2.4. Evaluation Index

To evaluate the precision and dependability of the diverse deep learning models in predicting performance, this study employs the subsequent assessment metrics: root mean square error (*RMSE*), mean absolute error (*MAE*), and coefficient of determination (R^2). The definitions of these three evaluation metrics are elaborated as per references [57,58]:

(1) Root mean square error (*RMSE*)

$$RMSE = \sqrt{\frac{1}{n}\sum_{i=1}^{n}(y_i - \hat{y}_i)^2} \tag{11}$$

(2) Mean absolute error (*MAE*)

$$MAE = \frac{1}{n}\sum_{i=1}^{n}|(y_i - \hat{y}_i)| \tag{12}$$

(3) Coefficient of determination (R^2)

$$R^2 = 1 - \frac{\sum_{i=1}^{n}(y_i - \hat{y}_i)^2}{\sum_{i=1}^{n}(y_i - \overline{y})^2} \tag{13}$$

where y_i represents the actual values of sea level, $\hat{y}_i$ represents the values predicted by each model, $\overline{y}$ is the mean of the actual values of sea level, and n denotes the total number of data points related to sea level. For *RMSE* and *MAE*, smaller values indicate higher predictive accuracy, while for R^2, values closer to 1 indicate accurate predictions and values closer to 0 suggest that the model has weaker explanatory power.

To compare the enhanced performance of the VMD-EEMD-LSTM model with other hybrid models using various accuracy evaluation metrics, this study introduces the concept of an improvement ratio (*I*). By computing *I*, we can accurately quantify the degree of improvement achieved by the VMD-EEMD-LSTM model in terms of accuracy. The formula for calculating I is as follows:

$$I_{y\hat{y}} = \frac{y - \hat{y}}{y} \tag{14}$$

where y and $\hat{y}$ signify diverse evaluation metrics, y represents the evaluation metric of the hybrid models compared against the VMD–EEMD–LSTM model, while $\hat{y}$ represents the evaluation metric of the VMD–EEMD–LSTM model. If $I_{y\hat{y}}$ is greater than 0, it indicates a decreasing trend in the accuracy. If $I_{y\hat{y}}$ is less than 0, it indicates an increasing trend. The greater the absolute value of $|I_{y\hat{y}}|$, the greater the improvement in that evaluation metric for the hybrid model and vice versa.

3. Data and Experiments

3.1. Data Preprocessing

The satellite altimetry grid data used in this study were obtained from the European Union's Copernicus Earth Observation Program, specifically from the GLORYS12V1 product (GLOBAL_MULTIYEAR_PHY_001_030). The data have a spatial resolution of 0.083° × 0.083° and a temporal resolution of 1 day [59,60]. The GLORYS12V1 product is a reanalysis of the global ocean with a 1/12° horizontal resolution and 50 vertical levels, covering sea level measurements from 1993 onwards. It has undergone the necessary standard corrections [61].

In the process of selecting experimental data, we primarily adhere to the following requirements: (1) to ensure enough training data, the chosen sites should have the same and extensive time span, specifically covering daily data from 1993 to 2020, totaling 28 years. (2) In order to minimize the adverse impact of data missingness on model predictions, we stipulate that the selected station's data missing rate should not exceed 1%, and the lower the missing rate, the better. In accordance with these criteria, the selected sites are mainly distributed in the Netherlands. Given the low-lying topography within the Netherlands, approximately one-third of the country's land is situated below the average sea level [62]. The impact of sea level rise is profound in the Netherlands, underscoring the critical importance of accurate sea level predictions for the region. Therefore, we selected data from six satellite altimetry grid points near the Dutch coast as the experimental dataset. The latitude and longitude information of the data is shown in Table 1, and the distribution of the data can be observed in Figure 3.

Table 1. Details the of satellite altimetry data (the virtual coast altimetry stations are a satellite altimetry sequence solved on the basis of the latitude and longitude of the nearest tide gauge station to the coast).

Virtual Coastal Altimetry Station	ID	Longitude (°)	Latitude (°)	Deletion Rates (%)	Time Span (Years)
Maassluis	09	4.25	51.92	0	1993.0–2020.9
Vlissingen	20	3.60	51.44	0	1993.0–2020.9
Hoek Van Holland	22	4.12	51.98	0	1993.0–2020.9
Delfzijl	23	4.75	52.96	0	1993.0–2020.9
Harlingen	25	5.41	53.18	0	1993.0–2020.9
IJmuiden	32	4.56	52.46	0	1993.0–2020.9

To conduct a comprehensive analysis of the distribution of selected virtual coast altimetry station data, we have generated box plots for daily data for comparative analysis. The results are illustrated in Figure 4.

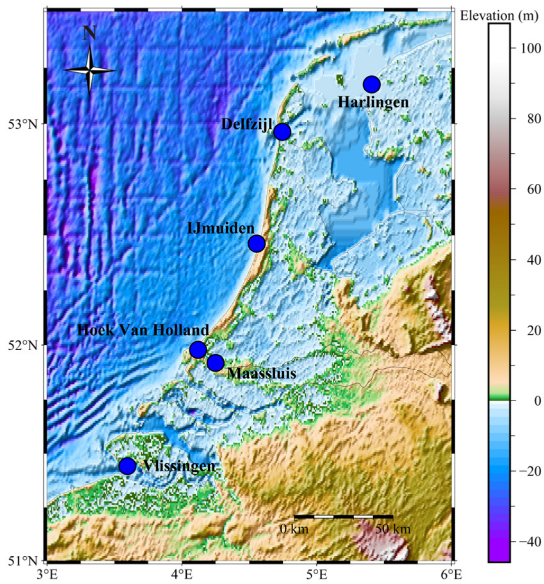

Figure 3. Distribution of virtual coast altimetry stations.

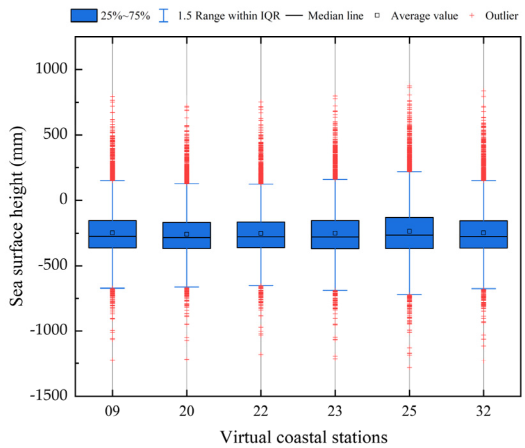

Figure 4. Box plots of virtual coast altimetry station data (25% and 75% represent the first and third quartiles, respectively, and IQR represents the interquartile range).

As can be seen from the box plots, since all selected experimental stations are located in the Netherlands, the distribution of sea level data is generally similar across the stations although there are differences in the presence of IQRs and anomalies. The site distribution map reveals that, despite the close proximity of the Maassluis and Hoek Van Holland sites, there are still noticeable differences in the data. Taking into consideration various factors, this divergence may be attributed to variances in the water circulation at river mouths and in the open sea. The Hoek Van Holland site, being close to the open sea, is significantly influenced by marine water circulation, while the Maassluis site, situated within a river, is more impacted by estuarine water circulation [63].

3.2. Experimental Pretreatment

3.2.1. Parameter Settings of VMD

Unlike EMD and EEMD, VMD allows for the autonomous selection of the number of mode components obtained during decomposition. This means that, when using VMD for data decomposition, it is crucial to choose the appropriate number of mode components, referred to as K, to achieve high-quality decomposition results. Choosing a K value that is too large can cause over-decomposition, while selecting one that is too small may lead to under-decomposition. In order to determine the best K value for the decomposition of the sea level height time series, this study uses the signal-to-noise ratio (SNR) as a measure of decomposition quality. A higher SNR means that the signal decomposition is more clear and the noise removal is better. After conducting thorough experiments and making empirical observations, this study limits the selection of K values to a range of 2 to 10. It also identifies the K value within this range that produces the highest SNR as the optimal K value for each individual time series [64,65].

$$\mathrm{SNR} = 10\lg\frac{\sum_{i=1}^{N} m^2(i)}{\sum_{i=1}^{N} [m(i) - n(i)]^2} \tag{15}$$

where $m(i)$ represents the original signal, and $n(i)$ represents the reconstructed signal. In VMD, the penalty factor α also exerts a certain influence on the decomposition outcomes. Given that the optimal range for the penalty factor α is typically between 1.5 and 2 times the size of the decomposed data [66], and to ensure experimental consistency while considering the size of the decomposed data in the experiments, this study set the penalty factor to 15,000 for all decomposition processes.

Because the range of virtual coast altimetry stations covered in this study was relatively small, the frequency of fluctuation and the amplitude of the sequences of sea level height were quite similar. Therefore, the optimal parameters obtained in the experiments were consistent, all indicating that K = 5 was the best number of components for decomposition (Figure 6 in Section 4.2 shows the results VMD for K = 5). To reduce the complexity of the subsequent experiments and ensure experimental consistency, this study combined the data with a K greater than 5 from the IMFs obtained by EMD and EEMD with the residual term for a better predictive analysis.

To further validate the reliability of the selected K value, the LSTM model was employed to conduct comparative experiments for sea level data prediction at the Maassluis station. The experimental results are presented in Table 2.

As presented in Table 2, distinct values of K in VMD produce residual sequences that manifest substantial predictive errors, constituting the primary source of discrepancies within the VMD-LSTM model. A comparative analysis of predictive outcomes across varying K values reveals that with the escalation of K, the R^2 for residual sequence predictions gradually diminishes, while the cumulative errors for each IMF increase. This observation implies that the selection of an excessively diminutive K value may result in an inadequate decomposition of the signal, ultimately yielding inferior predictive performance. Conversely, opting for an excessively large K value may lead to an exorbitant decomposition of the signal, which is also not conducive to model prediction.

When K is set at 5, the VMD-LSTM model attains the highest level of predictive accuracy. This reaffirms that, in the context of time series prediction for sea level data, K = 5 represents the optimal number of decompositions for VMD.

3.2.2. Parameter Settings of the Model

In deep learning prediction models, a variety of different parameters are involved, and the sizes of the parameters have different degrees of influence on the model's predictive accuracy. To ensure the reliability, this study conducted an experiment by setting the same model parameters. The configuration details of each model are presented in Table 3. In this experimental setup, the parameters for the LSTM model and the hybrid models were set to identical sizes.

Table 2. Prediction accuracy of VMD-LSTM model under different K value decompositions. (VMD$_K$-LSTM (K = 3, 4, 5, 6, 7) is a prediction model obtained by VMD under this K value).

Model	Series	*RMSE* (mm)	*MAE* (mm)	R^2
VMD$_3$-LSTM	IMF$_1$	0.5	0.4	1.0
	IMF$_2$	0.9	0.6	1.0
	IMF$_3$	1.3	1.0	1.0
	Residual	125.6	91.0	0.3
	All	**125.4**	**90.8**	**0.5**
VMD$_4$-LSTM	IMF$_1$	0.5	0.4	1.0
	IMF$_2$	0.6	0.5	1.0
	IMF$_3$	1.7	1.3	1.0
	IMF$_4$	1.0	0.8	1.0
	Residual	118.5	86.1	0.2
	All	**118.3**	**85.8**	**0.6**
VMD$_5$-LSTM	IMF$_1$	0.5	0.4	1.0
	IMF$_2$	0.6	0.4	1.0
	IMF$_3$	0.8	0.6	1.0
	IMF$_4$	1.6	1.2	1.0
	IMF$_5$	0.7	0.5	1.0
	Residual	114.7	83.5	0.2
	All	**114.3**	**83.1**	**0.6**
VMD$_6$-LSTM	IMF$_1$	0.4	0.3	1.0
	IMF$_2$	0.6	0.4	1.0
	IMF$_3$	0.8	0.6	1.0
	IMF$_4$	1.7	1.3	1.0
	IMF$_5$	1.2	0.9	1.0
	IMF$_6$	0.7	0.5	1.0
	Residual	115.1	85.3	0.2
	All	**115.0**	**85.1**	**0.6**
VMD$_7$-LSTM	IMF$_1$	0.5	0.4	1.0
	IMF$_2$	0.6	0.4	1.0
	IMF$_3$	0.6	0.4	1.0
	IMF$_4$	0.7	0.6	1.0
	IMF$_5$	1.7	1.3	1.0
	IMF$_6$	1.0	0.7	1.0
	IMF$_7$	0.6	0.4	1.0
	Residual	111.8	83.8	0.0
	All	**114.8**	**86.1**	**0.6**

Table 3. Hyperparameter settings for each model.

Model	ANN	RNN	GRU	LSTM	Instructions
Training set	7305	7305	7305	7305	Training data for model training (1993–2012)
Validation set	1095	1095	1095	1095	Validation data for tuning the hyperparameters and preventing overfitting (2012–2015)
Test set	1827	1827	1827	1827	Testing data for evaluating the model's performance (2015–2020)
Epochs	50	50	50	50	Number of iterations of the model
Learning rate	0.001	0.001	0.001	0.001	Hyperparameter controlling the step size of the updates of the model's parameters
Input_size	1	1	1	1	Dimensionality of the input layer
Output_size	1	1	1	1	Dimensionality of the output layer
Hidden_size	256	256	256	256	Dimensionality of the hidden layer
Seq_len	12	12	12	12	Length of each sliding data window
Batch_size	16	16	16	16	Batch size for one-time input in the time series data

According to the deep learning prediction model dataset division requirements, the dataset is divided according to 8:1:1 [67]. In order to better comprehensively evaluate the prediction performance of the model, this study has been adjusted on the basis of 8:1:1. All models use a unified data division scheme: 1993.0–2012.9 is the training set, 2012.9–2015.9 is the verification set, and 2015.9–2020.9 is the test set. The main purpose is to ensure that the model can have enough data for model testing under sufficient training sets to conduct a more comprehensive evaluation of the model's prediction performance.

4. Results and Analysis

4.1. Analysis of the Predictions of a Single Deep Learning Model

This section comprehensively evaluates and compares the predictive performance of four different models: ANN [68], RNN [69], gated recurrent units (GRUs) [70], and LSTM. Three different sequences of sea level height are used for the evaluation. The objective is to identify the model that performs best in time series forecasting, which will establish a reliable foundation for constructing the subsequent hybrid models. Figure 5 presents the precise evaluation metrics for the predictions made by each model.

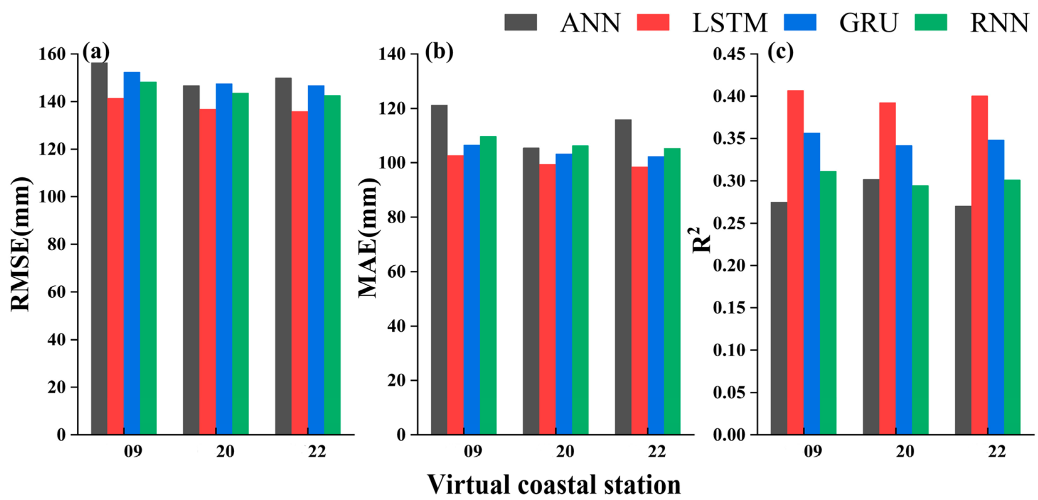

Figure 5. Comparison of the evaluation indicators of each model at different virtual coast altimetry stations (where 09, 20, and 22 are the ID numbers of the Maassluis, Vlissingen, and Hoek Van Holland virtual coast altimetry stations. Subfigure (**a**), (**b**), and (**c**) represent the accuracy evaluation indicators *RMSE*, *MAE*, and R^2, respectively).

As shown in Figure 5, for the three different time series datasets of sea level height, the ANN model exhibited the poorest predictive performance, with an average *RMSE* (the average *RMSE* of the analyzed sites) of 150.9 mm, an average *MAE* of 114.1 mm, and an average R^2 of 0.3 across the different monitoring stations. In contrast, the LSTM model performed the best, with an average *RMSE* of 137.9 mm, an average *MAE* of 100.1 mm, and an average R^2 of 0.4 across the different monitoring stations. LSTM outperformed ANN, RNN, and GRU, demonstrating its superiority. However, since LSTM is a single model, it failed to fully extract the features of the data during training, resulting in a relatively high *RMSE* and *MAE* and a relatively low R^2 for the predictions. This phenomenon highlights the challenge that single models face in accurately capturing all the fluctuations and trends in time series data, especially in complex time series forecasting tasks. Therefore, in the subsequent work of constructing the hybrid models, it is necessary to combine the characteristics of the data decomposition methods to further improve the predictive accuracy of the models.

4.2. Analysis of the Hybrid Deep Learning First-Order Decomposition Model

In response to the issue of insufficient extraction of the features of the data by single models in complex time series forecasting, this study introduced and compared four different data decomposition methods: VMD, EMD, EEMD, and CEEMDAN. Taking the original sea level data from the Maassluis station as an example, these methods decomposed the data into multiple IMFs and a residual sequence. Subsequently, the decomposed sequences were used as the model's features and individually fed into the LSTM model for making predictions. The results for each IMF and residual sequence are shown in Figures 6 and 7. This experiment aimed to gain a deeper understanding of how the different data decomposition methods impact the performance of the LSTM model and evaluated their potential for improving the accuracy of time series predictions.

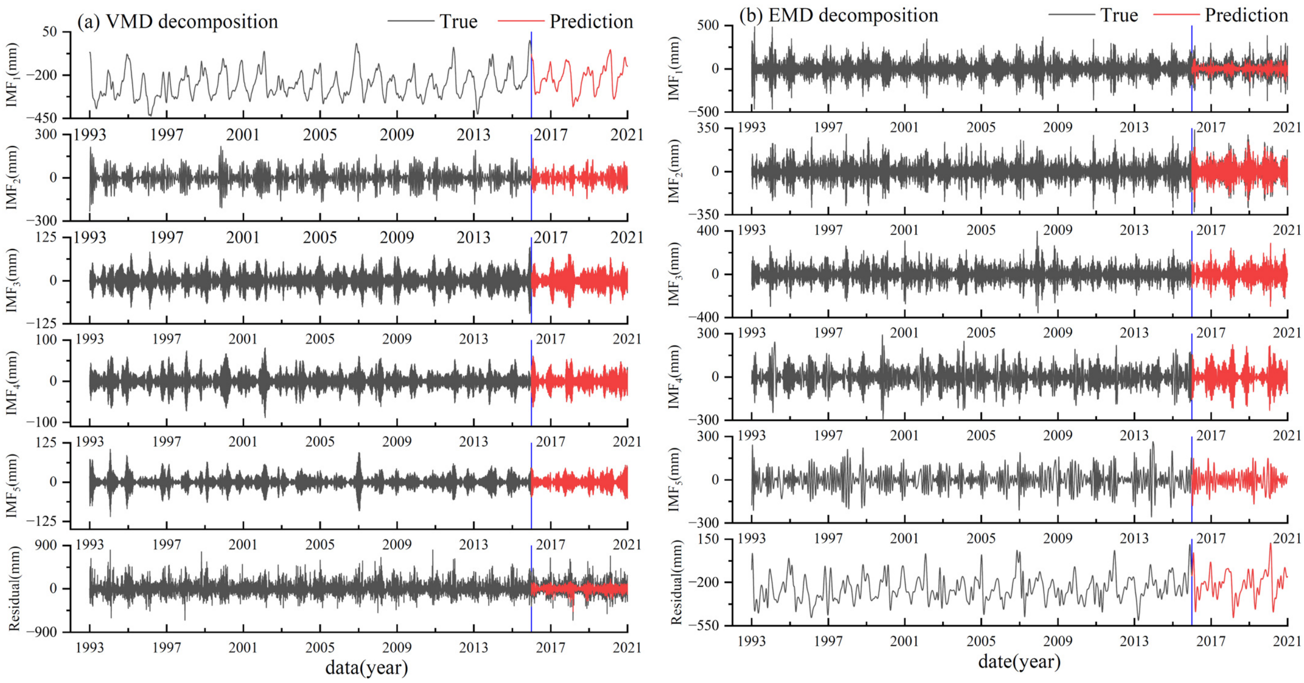

Figure 6. Predictions of IMF and residual series under VMD (**a**) and EMD (**b**). (The result after the blue vertical line is the test set).

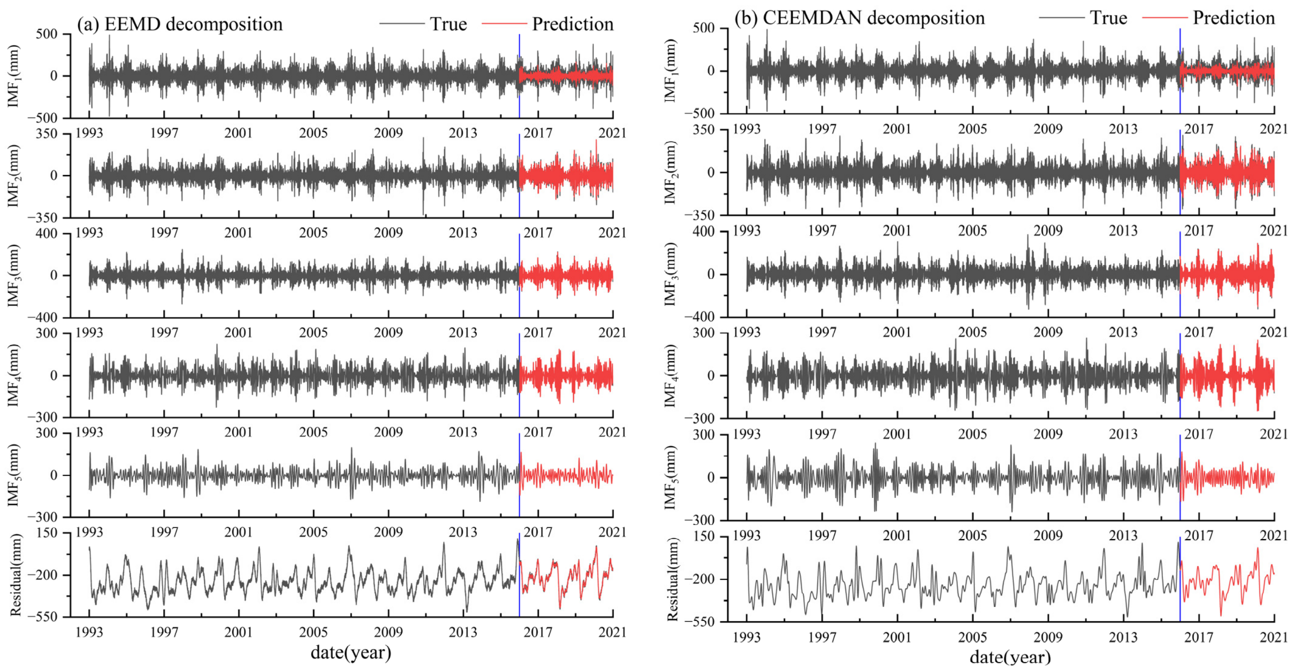

Figure 7. Predictions of IMF and residual series under EEMD (**a**) and CEEMDAN (**b**). (The result after the blue vertical line is the test set).

In Figures 6 and 7, the "Residual" presented for EMD, EEMD, and CEEMDAN refers to the results obtained by adding up the various IMFs after IMF_5 and the residual sequence. From the figures, it can be observed that the IMFs obtained after VMD have well-defined frequency signals and waveform characteristics. Therefore, the LSTM model produced excellent predictions for each IMF. However, the residual sequence generated after VMD was relatively large and contained a significant amount of white noise. Consequently, even though there were some waveform features and patterns in the residual sequence, they were challenging for the LSTM model to capture, resulting in less accurate predictions, subsequently affecting the overall accuracy of the VMD–LSTM model's predictions. In contrast, the EMD, EEMD, and CEEMDAN methods, while not performing as well as VMD for predicting the various IMFs, yielded better prediction results for the residual sequence. In order to analyze the accuracy of the predictions, this study summarized the evaluation metrics of each hybrid model's results, as shown in Table 4.

Table 4. Summary of each evaluation index of the accuracy of the time series predictions of different decomposition methods.

Model	Series	*RMSE* (mm)	*MAE* (mm)	R^2
VMD-LSTM	IMF_1	0.5	0.4	1.0
	IMF_2	0.6	0.4	1.0
	IMF_3	0.8	0.6	1.0
	IMF_4	1.6	1.2	1.0
	IMF_5	0.7	0.5	1.0
	Residual	114.7	83.5	0.2
	All	**114.3**	**83.1**	**0.6**
EMD-LSTM	IMF_1	76.6	58.4	0.2
	IMF_2	34.3	23.5	0.8
	IMF_3	7.3	4.8	1.0
	IMF_4	1.1	0.6	1.0
	IMF_5	0.4	0.3	1.0
	Residual	0.8	0.5	1.0
	All	**82.4**	**61.4**	**0.8**
EEMD-LSTM	IMF_1	63.0	46.0	0.3
	IMF_2	17.6	11.9	0.9
	IMF_3	2.7	1.9	1.0
	IMF_4	0.5	0.3	1.0
	IMF_5	0.3	0.2	1.0
	Residual	12.2	9.7	1.0
	All	**65.0**	**47.2**	**0.9**
CEEMDAN-LSTM	IMF_1	76.9	58.1	0.2
	IMF_2	33.5	23.1	0.8
	IMF_3	6.9	4.5	1.0
	IMF_4	1.1	0.7	1.0
	IMF_5	0.4	0.3	1.0
	Residual	0.4	0.3	1.0
	All	**82.8**	**61.2**	**0.8**

Based on the data presented in Table 4, it is clear that the EEMD-LSTM model outperformed the other models in terms of overall predictive accuracy. The EMD-LSTM model and the CEEMDAN model performed well, but slightly less well than the EEMD-LSTM model. On the other hand, the VMD-LSTM model had the lowest predictive accuracy. However, it should be noted that a significant portion of the prediction errors in the VMD-LSTM model were attributed to the predictions of the residual sequence. Additionally, the prediction errors for the different IMFs were considerably lower compared to those of the EMD-LSTM, EEMD-LSTM, and CEEMDAN models.

Although the EEMD-LSTM model may have lower predictive accuracy for the residual sequence compared to the EMD-LSTM and CEEMDAN models, it excels in IMF prediction accuracy and overall accuracy. The CEEMDAN method, despite its enhanced robustness and applicability compared to EMD, yields predictive accuracy similar to that of the EMD-LSTM model. This implies that the CEEMDAN-LSTM model does not significantly improve predictive performance in high-resolution sea level data compared to the EMD-LSTM model.

While the EEMD–LSTM model did not perform as strongly as the EMD–LSTM model in forecasting the residual sequence, it outperformed the EMD–LSTM model in forecasting the IMFs. As a result, the VMD–LSTM model excelled in IMF prediction, whereas the EEMD–LSTM model exhibited the highest overall predictive accuracy. Building upon these insights, this study introduced the VMD–EEMD–LSTM model, which enhances overall predictive accuracy by reprocessing the residual components obtained from VMD with EEMD in addition to the VMD–LSTM model.

4.3. Analysis of the Predictions of the Mixed VMD–EEMD–LSTM Second-Order Decomposition Model

In order to thoroughly assess the predictive performance of the VMD–EEMD–LSTM model compared to the VMD–LSTM and EEMD–LSTM models, this study conducted comparative experiments using sea level data from six different monitoring stations (Maassluis, Vlissingen, Hoek Van Holland, Delfzijl, Harlingen, IJmuiden). In this section, Maassluis station is taken as an example to analyze the differences in the predictions of the hybrid models. To distinguish the model prediction results more clearly, this section introduces the prediction error R to better analyze the differences between the predictions of each hybrid model and the original data (where R is defined as the difference between the model prediction results and the corresponding original data). The comparative results are shown in Figure 8.

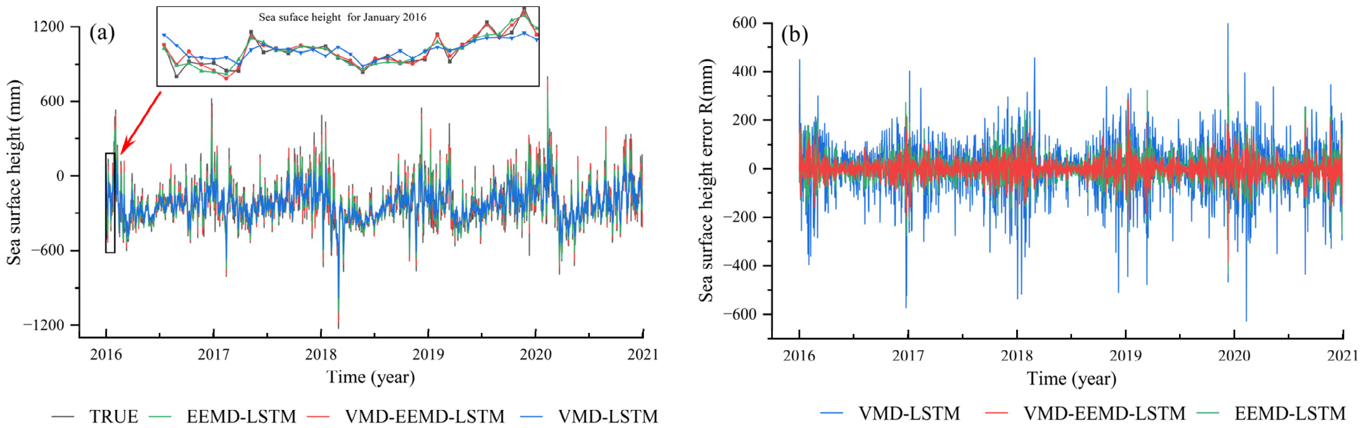

Figure 8. Predictions and errors of each mixed model (TRUE in the figure is the original time series of sea surface height. (**a**) depicts the prediction results for the mixed models at the Maassluis station sea surface height, while (**b**) illustrates the prediction error R generated by the mixed models at the same station. The enlarged area in (**a**) shows the comparison of the models' predictions for the first month of 2016 at Maassluis station.

As depicted in Figure 8, the magnified prediction results for January 2016 clearly indicate that the VMD-EEMD-LSTM model exhibits a good fitting performance with the original sequence. While the VMD-LSTM model maintains consistency with the original sequence in terms of fluctuation trends, it shows a certain gap in prediction accuracy compared to other hybrid models. Although the EEMD-LSTM model outperforms the VMD-LSTM model in terms of fluctuation trends, the fitting results of EEMD-LSTM are still not as favorable as those of the VMD-EEMD-LSTM model.

From the overall prediction results, it can be concluded that the VMD-LSTM model, while reasonably aligning with the overall trend of sea level fluctuations, exhibited sub-optimal performance near extreme points, particularly in proximity to local maxima. This observation suggests that the VMD–LSTM model struggled to capture the nuanced characteristics of sea level fluctuations, leading to notable prediction errors. In contrast, the EEMD-LSTM model's predictions closely match the original data, notably in capturing the amplitude of fluctuations, which significantly outperformed those of the VMD–LSTM model. Nevertheless, on a comprehensive scale, the results achieved by the EEMD–LSTM model still lagged behind those of the VMD–EEMD–LSTM model. This indicates that the VMD–EEMD–LSTM model not only represents an enhancement over the VMD–LSTM model but also surpasses the EEMD–LSTM model in predictive accuracy. It underscores the effectiveness of this hybrid model in combining the predictive strengths of the VMD–LSTM and EEMD–LSTM models, resulting in superior outcomes and overall improved predictive performance.

4.4. Analysis of the Accuracy of the Predictions of the Mixed VMD–EEMD–LSTM Second-Order Decomposition Model

4.4.1. Analysis of the Results of the Evaluation Index

To gain a more precise insight into the enhancement achieved by the VMD–EEMD–LSTM model in comparison to the VMD–LSTM and EEMD–LSTM models across diverse time series, this section scrutinizes the *RMSE*, *MAE*, and R^2 of the predictions made by the three hybrid models for sea level time series data collected from six different stations. Figure 9 displays the accuracy evaluation indexes for different hybrid model predictions at individual stations, while Table 5 presents the improvement ratio in the accuracy of the VMD-EEMD-LSTM model compared to the VMD-LSTM model and the EEMD-LSTM model.

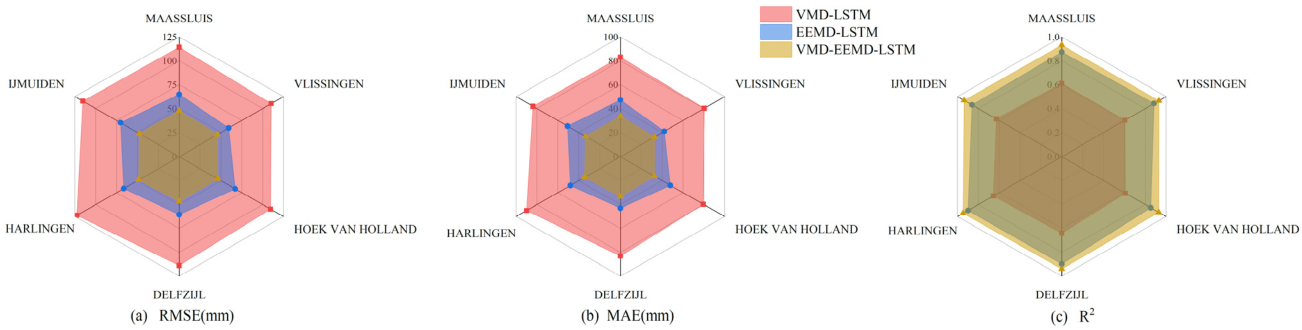

Figure 9. Evaluation indexes for accuracy assessment of various hybrid model predictions at each station (red, blue, and yellow dots and areas represent accuracy assessment indexes for the VMD-LSTM model, EEMD-LSTM model, and VMD-EEMD-LSTM model, respectively, at each station; (**a**) depicts the *RMSE* values, (**b**) illustrates the *MAE* values, and (**c**) displays R^2 values for hybrid model predictions across different virtual coast altimetry stations).

Figure 9 demonstrates that both the VMD-EEMD-LSTM model and the EEMD-LSTM model exhibit markedly superior predictive accuracy in comparison to the VMD-LSTM model. Furthermore, the VMD-EEMD-LSTM model showcases a noticeable degree of enhancement over the EEMD-LSTM model. The three hybrid models consistently demonstrated similar performance when predicting accuracy across various stations. This suggests that the sea level heights observed at the selected stations in the Netherlands displayed a degree of consistency, resulting in relatively minor variations in prediction accuracy. However, in comparison to the VMD–EEMD–LSTM model, the EEMD–LSTM model exhibited some fluctuations in the evaluation metrics across different time series predictions. This signifies that the stability and accuracy of the EEMD–LSTM model in forecasting results for diverse time series are not as robust as those of the VMD–EEMD–LSTM model. This result underlines the superiority of the VMD–EEMD–LSTM model in handling time series from different stations and, to some extent, validates its ability to adapt more stably to various requirements and scenarios of prediction.

Table 5. Evaluation indexes for hybrid model accuracy at different virtual coast altimetry stations and accuracy improvement of VMD-EEMD-LSTM model (the improvement in accuracy of the VMD-EEMD-LSTM model over the VMD-LSTM model is denoted by I1, while I2 represents the corresponding improvement over the EEMD-LSTM model).

Virtual Coast Altimetry Station	Evaluation Index	Prediction Model			Improvement Ratio (I)	
		VMD-LSTM	EEMD-LSTM	VMD-EEMD-LSTM	I_1 (%)	I_2 (%)
Maassluis	*RMSE* (mm)	114.3	65.0	47.8	58.2	26.5
Vlissingen		110.3	59.4	46.0	58.3	22.5
Hoek Van Holland		109.5	67.1	46.3	57.7	31.0
Delfzijl		113.9	60.6	46.9	58.9	22.6
Harlingen		122.7	66.5	48.4	60.5	27.1
IJmuiden		115.4	70.3	47.8	58.6	32.0
Maassluis	*MAE* (mm)	83.1	47.2	33.6	59.6	28.9
Vlissingen		80.3	42.0	32.7	59.3	22.2
Hoek Van Holland		79.5	47.9	32.6	59.1	32.0
Delfzijl		83.1	43.0	33.2	60.0	22.8
Harlingen		90.0	48.0	34.4	61.8	28.3
IJmuiden		83.8	50.7	33.6	60.0	33.8
Maassluis	R^2	0.6	0.9	0.9	−52.5	−6.6
Vlissingen		0.6	0.9	0.9	−54.0	−5.2
Hoek Van Holland		0.6	0.9	0.9	−52.5	−9.0
Delfzijl		0.6	0.9	0.9	−46.6	−4.5
Harlingen		0.7	0.9	1.0	−44.2	−5.3
IJmuiden		0.6	0.9	0.9	−49.3	−8.6

Table 5 demonstrates that the VMD-EEMD-LSTM model consistently exhibits high prediction accuracy (*RMSE* = 47.21 mm, *MAE* = 33.3 mm, R^2 = 0.9) across various stations. In comparison to both the VMD-LSTM and EEMD-LSTM models, accuracy evaluation indexes exhibit significant improvements. Compared to the EEMD-LSTM model, the VMD-EEMD-LSTM model achieved an average reduction of 27.0% in *RMSE*, 28.0% in *MAE*, and an average improvement of 6.5% in R^2. The EEMD–LSTM model showed a relatively modest increase of only 6.5% in the R^2, indicating that it could fit the actual distribution of the data well. The limited improvement in R^2 for the EEMD–LSTM model also indirectly confirmed the high predictive accuracy and superior performance of the VMD–EEMD–LSTM model.

Compared with the VMD–LSTM model, the VMD–EEMD–LSTM model exhibited even more significant improvements in the accuracy of its prediction, with an average reduction of 58.7% in the *RMSE*, an average reduction of 60.0% in the *MAE*, and an average increase of 49.9% in the R^2. This demonstrates that in practical VMD–LSTM predictions, there is significant room for improvement due to the incomplete decomposition of VMD.

4.4.2. Comparison of the Trend from Satellite Altimetry and Tide Gauge Observations

To further explore the effectiveness of the proposed VMD-EEMD-LSTM model in predicting sea surface height (SSH), we combine the model's prediction results with satellite altimetry data from the training and validation sets. This fusion results in a combined satellite altimetry dataset, which is then compared with tidal gauge (TG) observational data for the corresponding time periods. Using an autoregressive fractionally integrated moving average (ARFIMA) (1, d, 1) noise model [71], we calculate the velocity and vertical land motion (VLM) corrections, with the detailed outcomes presented in Table 6.

Table 6. Comparison of velocities from satellite altimetry and tide gauge observations (V_{TG} and V_{SSH} represent the velocities calculated by TG and SSH, respectively, in mm/year).

Virtual Coastal Altimetry Station	V_{TG}	Co-GNSS	Distance (km)	*VLM* at Co-GNSS	$V_{TG} + VLM$	V_{SSH}	$\lvert V_{TG} + VLM - V_{SSH} \rvert$
Maassluis	2.26	dlf1	11.90	−0.47	1.79	2.20	0.41
Vlissingen	2.97	vlis	0.40	−0.80	2.17	2.10	0.07
Hoek Van Holland	2.43	hhol	10.70	−0.45	1.97	2.32	0.34
Delfzijl	2.08	txe2	11.30	−0.33	1.75	2.42	0.67
Harlingen	3.56	ters	24.00	−1.11	2.45	2.34	0.11
IJmuiden	1.98	ijmu	0.40	−1.66	0.32	2.38	2.06

It can be seen from Table 6 that the trends obtained from satellite altimetry predictions generally align with those estimated by $V_{TG} + VLM$, and the $\lvert V_{TG} + VLM - V_{SSH} \rvert \leq 2$ for most of the sites, which indicates that the predicted V_{SSH} show a good consistency in the trend of tide gauge observations [72]. This further confirms the reliability of the time series predicted by our proposed VMD-EEMD-LSTM model. In summary, this study utilizes satellite altimetry data to estimate and forecast sea surface height. The findings indicate that the VMD-EEMD-LSTM model, which leverages the strengths of both hybrid prediction models, substantially enhances both predictive accuracy and the overall performance of sea surface height forecasts.

5. Discussion

Based on the comprehensive analysis of the obtained experimental results, we conclude that the hybrid deep learning prediction model constructed using the combination of VMD and EEMD methods possesses strong prediction performance and can significantly improve the prediction accuracy of the sea level time series. The LSTM model, as an excellent algorithm in neural networks, demonstrates notable advantages in predicting long-term time series, owing to its powerful memory function that contributes to outstanding predictive capabilities. However, due to the limitations of the LSTM model in feature extraction of complex time series, high-precision time series prediction still needs to use other methods to further extract data features [73].

Ban et al. (2023) successfully applied the VMD-LSTM model to long-term tidal height predictions and validated its superior performance compared to methods such as EMD, EEMD, and CEEMDAN [74]. However, the experimental results in this paper show that although the VMD-LSTM model exhibits excellent prediction accuracy on each IMF, there is a higher prediction error in the residual term prediction, which constitutes a significant source of prediction errors for the VMD-LSTM model. Therefore, if effective measures are not taken to address the errors in the residual sequence, the overall predictive accuracy of the VMD-LSTM model may be inferior to that of hybrid models such as EMD-LSTM.

In the field of ozone prediction, Tang et al. (2023) conducted a preliminary application of the VMD-EEMD-LSTM model and confirmed its high predictive accuracy. However, in their accuracy comparison, the study was limited to a comparison between EEMD-LSTM and VMD-EEMD-LSTM, without considering the predictive accuracy of the VMD-LSTM model. Additionally, a detailed comparative analysis of the predictive accuracy of IMFs and residual terms under various first-order hybrid models was not conducted. This limitation resulted in a relatively insufficient in-depth discussion of the predictive accuracy of the VMD-EEMD-LSTM model [75].

In the experiments conducted in this paper, a detailed comparative analysis of the predictive accuracy of four first-order hybrid models, namely VMD-LSTM, EMD-LSTM, EEMD-LSTM, and CEEMDAN-LSTM, was performed. Building on this analysis, the paper proposes a second-order hybrid prediction model, termed VMD-EEMD-LSTM, which combines the strengths of the VMD-LSTM and EEMD-LSTM models. Furthermore, by analyzing the sources of prediction errors in the EEMD-LSTM model, a fusion approach is introduced in the VMD-EEMD-LSTM model to integrate selected IMFs from the EEMD, thereby reducing the model complexity.

Due to the utilization of a second-order hybrid model for prediction in this study, the model complexity is inevitably higher than that of a first-order hybrid model. Additionally, different values of K in the VMD process have a significant impact on the decomposition results. Therefore, when conducting various prediction tasks, careful consideration of these factors is essential. In future research, to enhance model performance and robustness, the following aspects could be considered: (1) the performance of VMD, EMD, EEMD, and CEEMDAN may be sensitive to specific signal features and may exhibit varying performance for different data characteristics. Consequently, adjusting the decomposition methods according to different time series could lead to improved overall model performance. (2) During the VMD, different values of K and α may affect the results. Adjusting these parameters through parameter optimization methods holds the potential to enhance the accuracy of the decomposition and overall model performance. (3) The LSTM model used in this experiment, considering the issue of model complexity, adopted a basic model framework with a single layer and unidirectional structure. For more complex data prediction tasks, consideration could be given to adjusting model settings, such as increasing the number of layers or adopting a bidirectional structure, to improve the overall predictive performance of the model.

6. Conclusions

This article discusses a new method for the high-precision time series forecasting of sea level height based on VMD–LSTM, named VMD–EEMD–LSTM. It addresses the limitations in the VMD–LSTM model, such as the insufficient decomposition of VMD, and enhances the robustness compared with the EEMD–LSTM model. The method's reliability was validated using multiple experiments involving Dutch coastal satellite altimetry data. The key findings are as follows.

(1) By comparing the predictions of different individual models, it is evident that the LSTM model exhibits the best predictive performance. However, the average *RMSE* remains high at 137.9 mm, the average *MAE* is 100.1 mm, and the average R^2 is only 0.4 across different measurement stations. This indicates that single deep learning predictive models often suffer from insufficient feature extraction when dealing with complex time series data, resulting in generally lower predictive accuracy.

(2) Comparing the four hybrid prediction models, VMD-LSTM, EMD-LSTM, EEMD-LSTM, and CEEMDAN-LSTM, the VMD-LSTM model has the lowest predictive accuracy across different measurement stations, with an average *RMSE* of 111.3 mm, an average *MAE* of 81.0 mm, and an average R^2 of 0.6. In contrast, the EEMD-LSTM model demonstrates the highest predictive accuracy, with an average *RMSE* of 63.8 mm, an average *MAE* of 45.7 mm, and an average R^2 of 0.9. Although the VMD-LSTM model lags behind EMD-LSTM EEMD-LSTM and CEEMDAN-LSTM models in overall predictive accuracy, its individual IMF components exhibit exceptionally high predictive accuracy within the LSTM model. While the IMF components of the EEMD-LSTM model may not match the VMD-LSTM model in predictive accuracy, the overall predictive accuracy of EEMD-LSTM surpasses that of VMD-LSTM.

(3) In conclusion, through a comprehensive analysis of six sets of sea surface height data along the Dutch coast, our experimental results firmly validate the exceptional predictive accuracy of the VMD-EEMD-LSTM hybrid model proposed in this paper (*RMSE* = 47.2 mm, *MAE* = 33.3 mm, R^2 = 0.9). When compared to the VMD-LSTM model, we observe an average reduction in *RMSE* by 58.7% and *MAE* by 60.0% and an improvement in R^2 by 49.9%. Similarly, in comparison with the EEMD-LSTM model, we note an average reduction in *RMSE* by 27.0% and *MAE* by 28.0% and an improvement in R^2 by 6.5%. These results unequivocally demonstrate the significant enhancement in predictive accuracy of sea surface height time series, opening new

avenues for future research and affirming the model's potential for understanding and predicting sea level changes and related environmental phenomena.

Future studies may further explore the applicability of this hybrid model in different geographic regions and consider the incorporation of additional data sources to refine prediction accuracy.

In the future, the development of artificial intelligence algorithms could enable intelligent assessments of various parameter optimization methods, data decomposition techniques, and different hybrid approaches to deep learning prediction models. This intelligent evaluation process aims to select the optimal hybrid prediction model for complex time series forecasting tasks. Future research will predominantly focus on delving deeper into factors associated with sea level rise, including but not limited to glacier melting and sea water temperature. Additionally, the potential applications of this hybrid prediction model extend to other domains requiring high-precision time series predictions, such as weather and climate forecasting, stock forecasting, and forecasting in the energy sector.

Author Contributions: H.C. and J.H. writing—original draft preparation; X.H. and T.L. methodology, reviewing and editing the manuscript; H.C. and X.S. data processing and figure plotting. All authors have read and agreed to the published version of the manuscript.

Funding: This work was sponsored by National Natural Science Foundation of China (42364002, 42374040), Major Discipline Academic and Technical Leaders Training Program of Jiangxi Province (20225BCJ23014).

Data Availability Statement: The data presented in this study can be downloaded from this website: https://data.marine.copernicus.eu/product/GLOBAL_MULTIYEAR_PHY_001_030/description.

Conflicts of Interest: The authors declare no conflict of interest.

References

1. Cazenave, A.; Llovel, W. Contemporary Sea level rise. *Annu. Rev. Mar. Sci.* **2010**, *2*, 145–173. [CrossRef] [PubMed]
2. Nicholls, R.J.; Cazenave, A. Sea-level rise and its impact on coastal zones. *Science* **2010**, *328*, 1517–1520. [CrossRef] [PubMed]
3. IPCC. *Climate Change 2023: Synthesis Report. Contribution of Working Groups I, II and III to the Sixth Assessment Report of the Intergovernmental Panel on Climate Change*; IPCC: Geneva, Switzerland, 2023; pp. 35–115.
4. Titus, J.G.; Anderson, K.E. *Coastal Sensitivity to Sea-Level Rise: A Focus on the Mid-Atlantic Region*; Climate Change Science Program: Washinghton, DC, USA, 2009; Volume 4.
5. Cerqueira, V.; Torgo, L.; Soares, C. Machine learning vs statistical methods for time series forecasting: Size matters. *arXiv* **2019**, arXiv:1909.13316.
6. Bontempi, G.; Ben Taieb, S.; Le Borgne, Y.A. Machine learning strategies for time series forecasting. In *Business Intelligence: Second. European Summer School, eBISS 2012, Brussels, Belgium, 15–21 July 2012*; Tutorial Lectures 2; Springer: Berlin/Heidelberg, Germany, 2013; pp. 62–77.
7. Armstrong, J.S.; Collopy, F. *Integration of Statistical Methods and Judgment for Time Series Forecasting: Principles from Empirical Research*; John Wiley & Sons: Hoboken, NJ, USA, 1998; pp. 269–293.
8. Abraham, B.; Ledolter, J. *Statistical Methods for Forecasting*; John Wiley & Sons: Hoboken, NJ, USA, 2009.
9. Faruk, D.Ö. A hybrid neural network and ARIMA model for water quality time series prediction. *Eng. Appl. Artif. Intel.* **2010**, *23*, 586–594. [CrossRef]
10. Kalekar, P.S. Time series forecasting using holt-winters exponential smoothing. *Kanwal Rekhi Sch. Inf. Technol.* **2004**, *4329008*, 1–13.
11. Young, P.; Young, P. Alternative Recursive Approaches to Time-Series Analysis. In *Recursive Estimation and Time-Series Analysis: An Introduction*; Springer: Berlin/Heidelberg, Germany, 1984; pp. 205–230.
12. Adebiyi, A.A.; Adewumi, A.O.; Ayo, C.K. Comparison of ARIMA and artificial neural networks models for stock price prediction. *J. Appl. Math.* **2014**, *2014*, 614342. [CrossRef]
13. Masini, R.P.; Medeiros, M.C.; Mendes, E.F. Machine learning advances for time series forecasting. *J. Econ. Surv.* **2023**, *37*, 76–111. [CrossRef]
14. Sapankevych, N.I.; Sankar, R. Time series prediction using support vector machines: A survey. *IEEE Comput. Intell. Mag.* **2009**, *4*, 24–38. [CrossRef]
15. Lai, R.K.; Fan, C.Y.; Huang, W.H.; Chang, P.C. Evolving and clustering fuzzy decision tree for financial time series data forecasting. *Expert Syst. Appl.* **2009**, *36*, 3761–3773. [CrossRef]
16. Huang, S.; Wang, D.; Wu, X.; Tang, A. Dsanet: Dual self-attention network for multivariate time series forecasting. In Proceedings of the 28th ACM International Conference on Information and Knowledge Management, Beijing, China, 3–7 November 2019; pp. 2129–2132.

17. Tealab, A. Time series forecasting using artificial neural networks methodologies: A systematic review. *Future Comput. Inform. J.* **2018**, *3*, 334–340. [CrossRef]
18. Hajirahimi, Z.; Khashei, M. Hybrid structures in time series modeling and forecasting: A review. *Eng. Appl. Artif. Intell.* **2019**, *86*, 83–106. [CrossRef]
19. Di Nunno, F.; Granata, F.; Gargano, R.; de Marinis, G. Forecasting of extreme storm tide events using NARX neural network-based models. *Atmosphere* **2021**, *12*, 512. [CrossRef]
20. Granata, F.; Di Nunno, F. Neuroforecasting of daily streamflows in the UK for short-and medium-term horizons: A novel insight. *J. Hydrol.* **2023**, *624*, 129888. [CrossRef]
21. Di Nunno, F.; de Marinis, G.; Gargano, R.; Granata, F. Tide prediction in the Venice Lagoon using nonlinear autoregressive exogenous (NARX) neural network. *Water* **2021**, *13*, 1173. [CrossRef]
22. Shikhovtsev, A.Y.; Kovadlo, P.G.; Kiselev, A.V.; Eselevich, M.V.; Lukin, V.P. Application of Neural Networks to Estimation and Prediction of Seeing at the Large Solar Telescope Site. *Publ. Astron. Soc. Pac.* **2023**, *135*, 014503. [CrossRef]
23. Makarynskyy, O.; Makarynska, D.; Kuhn, M.; Featherstone, W.E. Predicting sea level variations with artificial neural networks at Hillarys Boat Harbour, Western Australia. Estuarine. *Estuar. Coast. Shelf S.* **2004**, *61*, 351–360. [CrossRef]
24. Nezhad, S.K.; Barooni, M.; Velioglu Sogut, D.; Weaver, R.J. Ensemble Neural Networks for the Development of Storm Surge Flood Modeling: A Comprehensive Review. *J. Mar. Sci. Eng.* **2023**, *11*, 2154. [CrossRef]
25. Alenezi, N.; Alsulaili, A.; Alkhalidi, M. Prediction of Sea Level in the Arabian Gulf Using Artificial Neural Networks. *J. Mar. Sci. Eng.* **2023**, *11*, 2052. [CrossRef]
26. Balogun, A.L.; Adebisi, N. Sea level prediction using ARIMA, SVR and LSTM neural network: Assessing the impact of ensemble Ocean-Atmospheric processes on models' accuracy. Geomatics. *Geomat. Nat. Haz Risk.* **2021**, *12*, 653–674. [CrossRef]
27. Lee, T. EMD and LSTM hybrid deep learning model for predicting sunspot number time series with a cyclic pattern. *Sol. Phys.* **2020**, *295*, 82. [CrossRef]
28. Yang, Y.; Yang, Y. Hybrid method for short-term time series forecasting based on EEMD. *IEEE Access* **2020**, *8*, 61915–61928. [CrossRef]
29. Zhu, Q.; Zhang, F.; Liu, S.; Wu, Y.; Wang, L. A hybrid VMD–BiGRU model for rubber futures time series forecasting. *Appl. Soft Comput.* **2019**, *84*, 105739. [CrossRef]
30. de Siqueira, B.V.P.; de Moraes Paiva, A. Using neural network to improve sea level prediction along the southeastern Brazilian coast. *Ocean Model.* **2021**, *168*, 101898. [CrossRef]
31. Song, C.; Chen, X.; Xia, W.; Ding, X.; Xu, C. Application of a novel signal decomposition prediction model in minute sea level prediction. *Ocean Eng.* **2022**, *260*, 111961. [CrossRef]
32. Wang, C.; Liu, Z.; Wei, H.; Chen, L.; Zhang, H. Hybrid deep learning model for short-term wind speed forecasting based on time series decomposition and gated recurrent unit. *Complex Syst. Model. Simul.* **2021**, *1*, 308–321. [CrossRef]
33. Dabbakuti, J.K.; Peesapati, R.; Kumar, A.K. Design and Development of Artificial Intelligence Enabled IoT Framework for Satellite Based Navigation Services. In *IEEE Transactions on Geoscience and Remote Sensing*; IEEE: New York, NY, USA, 2023.
34. Dabbakuti, J.R.K.K.; Jacob, A.; Veeravalli, V.R.; Kallakunta, R.K. Implementation of IoT analytics ionospheric forecasting system based on machine learning and ThingSpeak. *IET Radar Sonar Navig.* **2020**, *14*, 341–347. [CrossRef]
35. Wang, L.; Liu, Y.; Li, T.; Xie, X.; Chang, C. Short-term PV power prediction based on optimized VMD and LSTM. *IEEE Access* **2020**, *8*, 165849–165862. [CrossRef]
36. Huang, Y.; Yan, L.; Cheng, Y.; Qi, X.; Li, Z. Coal thickness prediction method based on VMD and LSTM. *Electronics* **2022**, *11*, 232. [CrossRef]
37. Han, L.; Zhang, R.; Wang, X.; Bao, A.; Jing, H. Multi-step wind power forecast based on VMD-LSTM. *IET Renew. Power Gen.* **2019**, *13*, 1690–1700. [CrossRef]
38. Dragomiretskiy, K.; Zosso, D. Variational mode decomposition. *IEEE Trans. Signal Process.* **2013**, *62*, 531–544. [CrossRef]
39. Rilling, G.; Flandrin, P.; Goncalves, P. On Empirical Mode Decomposition and Its Algorithms. In Proceedings of the IEEE-EURASIP Workshop on Nonlinear Signal and Image Processing, Antalya, Turkey, 20–23 June 2003; IEEE: New York, NY, USA, 2003; Volume 3, pp. 8–11.
40. Wu, Z.; Huang, N.E. Ensemble empirical mode decomposition: A noise-assisted data analysis method. *Adv. Adapt. Data Anal.* **2009**, *1*, 1–41. [CrossRef]
41. Lian, J.; Liu, Z.; Wang, H.; Dong, X. Adaptive variational mode decomposition method for signal processing based on mode characteristic. *Mech. Syst. Signal Process.* **2018**, *107*, 53–77. [CrossRef]
42. Pei, Y.; Wu, Y.; Jia, D. Research on PD signals denoising based on EMD method. *Prz. Elektrotechniczny* **2012**, *88*, 137–140.
43. Torres, M.E.; Colominas, M.A.; Schlotthauer, G.; Flandrin, P. A Complete Ensemble Empirical Mode Decomposition with Adaptive Noise. In Proceedings of the 2011 IEEE International Conference on Acoustics, Speech and Signal Processing (ICASSP), Prague, Czech Republic, 22–27 May 2011; IEEE: New York, NY, USA, 2011; pp. 4144–4147.
44. Wu, Z.; Huang, N.E.; Chen, X. The multi-dimensional ensemble empirical mode decomposition method. *Adv. Adapt. Data Anal.* **2009**, *1*, 339–372. [CrossRef]
45. Teja, K.; Tiwari, R.; Mohanty, S. Adaptive denoising of ECG using EMD, EEMD and CEEMDAN signal processing techniques. In *Journal of Physics: Conference Series*; IOP Publishing: New York, NY, USA, 2020; Volume 1706, p. 012077.

46. Graves, A.; Graves, A. Long short-term memory. In *Supervised Sequence Labelling with Recurrent Neural Networks*; Springer: Berlin/Heidelberg, Germany, 2012; pp. 37–45.
47. Chen, H.; Lu, T.; He, X.; Sun, X.; Huang, J.; Wang, J.; Yang, S. An improved DFVMD-LSTM hybrid time series model for predicting total solar irradiance. *Acta Geodyn. Geomater.* **2023**, *20*, 139–153. [CrossRef]
48. Sagheer, A.; Kotb, M. Time series forecasting of petroleum production using deep LSTM recurrent networks. *Neurocomputing* **2019**, *323*, 203–213. [CrossRef]
49. Gers, F.A.; Schmidhuber, J.; Cummins, F. Learning to forget: Continual prediction with LSTM. *Neural Comput.* **2000**, *12*, 2451–2471. [CrossRef] [PubMed]
50. Zhao, L.; Li, Z.; Qu, L.; Zhang, J.; Teng, B. A hybrid VMD-LSTM/GRU model to predict non-stationary and irregular waves on the east coast of China. *Ocean Eng.* **2023**, *276*, 114136. [CrossRef]
51. Yan, Y.; Wang, X.; Ren, F.; Shao, Z.; Tian, C. Wind speed prediction using a hybrid model of EEMD and LSTM considering seasonal features. *Energy Rep.* **2022**, *8*, 8965–8980. [CrossRef]
52. Liao, X.; Liu, Z.; Deng, W. Short-term wind speed multistep combined forecasting model based on two-stage decomposition and LSTM. J. *Wind Energy* **2021**, *24*, 991–1012. [CrossRef]
53. Jin, Y.; Guo, H.; Wang, J.; Song, A. A hybrid system based on LSTM for short-term power load forecasting. *Energies* **2020**, *13*, 6241. [CrossRef]
54. Chen, H.; Lu, T.; Huang, J.; He, X.; Yu, K.; Sun, X.; Ma, X.; Huang, Z. An Improved VMD-LSTM Model for Time-Varying GNSS Time Series Prediction with Temporally Correlated Noise. *Remote Sens.* **2023**, *15*, 3694. [CrossRef]
55. Li, Y.; Li, Y.; Chen, X.; Yu, J. Denoising and feature extraction algorithms using NPE combined with VMD and their applications in ship-radiated noise. *Symmetry* **2017**, *9*, 256. [CrossRef]
56. Li, C.; Wu, Y.; Lin, H.; Li, J.; Zhang, F.; Yang, Y. ECG denoising method based on an improved VMD algorithm. *IEEE Sens. J.* **2022**, *22*, 22725–22733. [CrossRef]
57. Chai, T.; Draxler, R.R. Root mean square error (RMSE) or mean absolute error (MAE)–Arguments against avoiding RMSE in the literature. *Geosci. Model Dev.* **2014**, *7*, 1247–1250. [CrossRef]
58. Ozer, D.J. Correlation and the coefficient of determination. *Psychol. Bull.* **1985**, *97*, 307. [CrossRef]
59. Belonenko, T.V.; Zinchenko, V.A.; Fedorov, A.M.; Budyansky, M.V.; Prants, S.V.; Uleysky, M.Y. Interaction of the Lofoten Vortex with a satellite cyclone. *Pure Appl. Geophys.* **2021**, *178*, 287–300. [CrossRef]
60. Feng, J.; Yuan, Y.; Zhang, T.; Zhang, Z.; Meng, D. Analysis of Ionospheric Anomalies before the Tonga Volcanic Eruption on 15 January 2022. *Remote Sens.* **2023**, *15*, 4879. [CrossRef]
61. Lellouche, J.M.; Greiner, E.; Le Galloudec, O.; Garric, G.; Regnier, C.; Drevillon, M.; Benkiran, M.; Testut, C.E.; Bourdalle-Badie, R.; Gasparin, F.; et al. Recent updates to the Copernicus Marine Service global ocean monitoring and forecasting real-time 1/12$\circ$ high-resolution system. *Ocean Sci.* **2018**, *14*, 1093–1126. [CrossRef]
62. Hoogland, T.; Van den Akker, J.J.H.; Brus, D.J. Modeling the subsidence of peat soils in the Dutch coastal area. *Geoderma* **2012**, *171*, 92–97. [CrossRef]
63. Montillet, J.P.; Melbourne, T.I.; Szeliga, W.M. GPS vertical land motion corrections to sea-level rise estimates in the Pacific Northwest. *J. Geophys. Res. Ocean.* **2018**, *123*, 1196–1212. [CrossRef]
64. Mei, L.; Li, S.; Zhang, C.; Han, M. Adaptive signal enhancement based on improved VMD-SVD for leak location in water-supply pipeline. *IEEE Sens. J.* **2021**, *21*, 24601–24612. [CrossRef]
65. Ding, M.; Shi, Z.; Du, B.; Wang, H.; Han, L. A signal de-noising method for a MEMS gyroscope based on improved VMD-WTD. *Meas. Sci. Technol.* **2021**, *32*, 095112. [CrossRef]
66. Ding, J.; Xiao, D.; Li, X. Gear fault diagnosis based on genetic mutation particle swarm optimization VMD and probabilistic neural network algorithm. *IEEE Access* **2020**, *8*, 18456–18474. [CrossRef]
67. Li, Y.; Wei, H.; Han, Z.; Huang, J.; Wang, W. Deep learning-based safety helmet detection in engineering management based on convolutional neural networks. *Adv. Civ. Eng.* **2020**, *2020*, 9703560. [CrossRef]
68. Wang, S.C.; Wang, S.C. Artificial neural network. In *Interdisciplinary Computing in Java Programming*; Springer: Berlin/Heidelberg, Germany, 2003; pp. 81–100.
69. Medsker, L.R.; Jain, L.C. Recurrent neural networks. In *Design and Applications*; CRC Press: Boca Raton, FL, USA, 2001; Volume 5, p. 2.
70. Dutta, A.; Kumar, S.; Basu, M. A gated recurrent unit approach to bitcoin price prediction. *J. Risk Financ. Manag.* **2020**, *13*, 23. [CrossRef]
71. He, X.; Montillet, J.P.; Fernandes, R.; Melbourne, T.I.; Jiang, W.; Huang, Z. Sea Level Rise Estimation on the Pacific Coast from Southern California to Vancouver Island. *Remote Sens.* **2022**, *14*, 4339. [CrossRef]
72. Bruni, S.; Fenoglio, L.; Raicich, F.; Zerbini, S. On the consistency of coastal sea-level measurements in the Mediterranean Sea from tide gauges and satellite radar altimetry. *J. Geod.* **2022**, *96*, 41. [CrossRef]
73. Widiputra, H.; Mailangkay, A.; Gautama, E. Multivariate cnn-lstm model for multiple parallel financial time-series prediction. *Complexity* **2021**, *2021*, 9903518. [CrossRef]

74. Ban, W.; Shen, L.; Lu, F.; Liu, X.; Pan, Y. Research on Long-Term Tidal-Height-Prediction-Based Decomposition Algorithms and Machine Learning Models. *Remote Sens.* **2023**, *15*, 3045. [CrossRef]
75. Tang, H.; Bhatti, U.A.; Li, J.; Marjan, S.; Baryalai, M.; Assam, M.; Ghadi, Y.Y.; Mohamed, H.G. A New Hybrid Forecasting Model Based on Dual Series Decomposition with Long-Term Short-Term Memory. *Int. J. Intell. Syst.* **2023**, *2023*, 9407104. [CrossRef]